ENVIRONMENTAL RESEARCH
LETTERS

LETTER

Unprecedented mass gain over the Antarctic ice sheet between 2021 and 2022 caused by large precipitation anomalies

Wei Wang[1], Yunzhong Shen[1,*], Qiujie Chen[1] and Fengwei Wang[2]

[1] College of Surveying and Geo-informatics, Tongji University, Shanghai, People's Republic of China
[2] State Key Laboratory of Marine Geology, Tongji University, Shanghai, People's Republic of China
[*] Author to whom any correspondence should be addressed.

E-mail: yzshen@tongji.edu.cn

Abstract

The Antarctic ice sheet (AIS) is susceptible to global climate change, and its mass loss has been 92 ± 18 Gt yr^{-1} between 1992 and 2020. Given the current intensive global warming, we investigate the AIS mass changes from January 2003 to December 2022, using the newly released satellite gravimetry and atmospheric datasets. The results show that the continuous mass loss in the AIS between 2003 and 2020 was 141.8 ± 55.6 Gt yr^{-1}. However, the AIS showed a record-breaking mass gain of 129.7 ± 69.6 Gt yr^{-1} between 2021 and 2022. During this period, the mass gain over the East AIS and Antarctic Peninsula was unprecedented within the past two decades, and it outpaced the mass loss in the Amundsen sector of the West AIS from 2003 to 2022. Basin-scale analysis shows that the mass gain mainly occurred over Wilhelm II Land, Queen Mary Land, Wilkes Land, and the Antarctic Peninsula due to anomalously enhanced precipitation. Further investigation reveals that during 2021–2022, a pair of symmetrically distributed high-low pressure systems, located at approximately 120°W and 60°E in the Southern Ocean, drove the observed abnormal precipitation and mass accumulation.

1. Introduction

The Antarctic ice sheet (AIS) melting has the potential to raise the global mean sea level (GMSL) by 58 m, and even a slight sea-level rise has direct societal and economic implications for coastal areas (Bars *et al* 2017, Oppenheimer *et al* 2019). Therefore, estimating its mass changes and understanding the driving factors is crucial. The AIS mass changes include SMB (surface mass balance) and ice dynamic processes. In the SMB, most ablation is from sublimation, and the important dynamic process is discharge across the grounding line. If the ice mass over the AIS is balanced, snowfall accumulation will balance surface ablation and ice discharge (Rignot *et al* 2019). However, numerous reports consistently indicate that the ice mass has been in imbalance, and they concur that ice mass loss over the AIS has outpaced gains from the mid-1990s through 2020 (The IMBIE team 2018). Specifically, the mass loss over the AIS contributed 7.4 ± 1.5 mm to GMSL from 1992 to 2020 (Otosaka *et al* 2022).

Mass changes over the AIS occur from decadal to interannual timescales (Li *et al* 2022). The interannual variations affect the estimation of long-term trends (Zhang *et al* 2020) and alter the short-term contribution to sea-level changes (Bodart and Bingham 2019). For instance, 350 Gt net ice gain over dronning Maud land (DML) from 2009 to 2011 is assessed by Boening *et al* (2012), which is equivalent to a decrease in GMSL rise at a rate of 0.32 mm yr^{-1} over the three years. Moreover, relative to the average change from 2002 to 2017, the extreme El Niño event resulted in a mass increase of 277 ± 91 Gt over the AIS between June 2015 and March 2017 (Bodart and Bingham 2019). The Amundsen Sea sector in the West AIS, the primary source of Antarctic mass loss, experienced a reduction in the total mass loss rate between 2019 and 2020 (Davison *et al* 2023). The elevation change records revealed a rapid mass loss in the Amundsen Sea sector from 2003 to 2021, while the mass loss slowed down between 2019 and 2021 (Yue *et al* 2023). Nonetheless, the mass balance over the entire AIS in the recent two years (2021–2022)

remains unclear. Given the intensive global warming and the impact of Antarctica on GMSL rise, it is imperative to extend the record of mass balance over the AIS and analyze the driving factors behind its short-term mass changes.

During the past decade, the mass balance record over the AIS has been significantly consolidated, benefiting from the data collected by the GRACE (Gravity Recovery and Climate Experiment) mission (Bamber *et al* 2018). As a successive mission, GRACE-FO (GRACE Follow-On) tracks changes in gravity since the end of the GRACE mission, allowing quantification of the cumulative mass change between the two missions (Sasgen *et al* 2020). With the GRACE and GRACE-FO observations, it has become possible to map the mass changes of the entire Antarctic over longer periods (Velicogna *et al* 2020). Therefore, in this study, we analyze the cumulative mass change characteristics over the AIS from January 2003 to December 2022 (20 years) and calculate the biennial mass change rate to demonstrate the short-term mass balance status. Then, we illustrate the geographical patterns of mass change and analyze the direct cause of the mass change. Finally, we reveal the basin-scale interannual mass variation and the primary driving factors.

2. Datasets and processing strategies

2.1. Study area
As defined by Zwally *et al* (2012), there are 27 drainage basins over the AIS (figure 1). These individual basins are then combined into three AIS regions (The IMBIE team 2018): East AIS (EAIS; Basins 2–17), West AIS (WAIS; Basins 1 and 18–23), and Antarctic Peninsula ice sheet (APIS; Basins 24–27).

2.2. GRACE/GRACE-FO data
Using the GRACE/GRACE-FO observations, the mascon (mass concentration) approach can estimate monthly cumulative mass anomalies relative to a given time at specific grid locations on the Earth's surface. Here, we used newly released 0.25 °× 0.25° mascon solutions (RL06, version 02) with an extended timespan provided by the CSR (Center for Space Research) at the University of Texas at Austin (Save 2020) to estimate mass changes over the AIS from January 2003 to December 2022. The CSR derives its mascon solutions with spherical harmonic coefficients up to degree and order of 120 (Save *et al* 2016) after the C_{20} (degree 2 order 0) coefficients and C_{30} (degree 3 order 0) coefficients for GRACE-FO period are replaced with those from SLR (Satellite Laser Ranging) (Loomis *et al* 2019, 2020) and the absent degree-1 coefficients are added with those from the Technical Note-13 (Save 2020). The glacial-isostatic adjustment (GIA) correction is completed with the ICE6G-D model (Peltier *et al* 2018).

2.3. Meteorological fields
The Regional Atmospheric Climate Model 2 (RACMO2), Version 2.3p2, with a spatial resolution of 27 km × 27 km, is used to estimate the SMB over the AIS from January 1979 to December 2022 (van Wessem *et al* 2018). Since there are potential errors and biases in particular precipitation datasets (González-Herrero *et al* 2023), the average of the precipitation fields from the RACMO2, Modern-Era Retrospective analysis for Research and Applications version 2 (MERRA-2; at 0.5° × 0.625° spatial resolution, Gelaro *et al* 2017), and the European Centre for Medium-Range Weather Forecasts Reanalysis version 5 (ERA5; at 0.25° × 0.25° spatial resolution, Hersbach and Dee 2016) reanalysis products is used to explore the relationship between the precipitation and the interannual mass variations over the AIS. The spatial resolutions of the RACMO2 and the precipitation fields are adjusted to match the resolution of CSR mascon solutions through spatial averaging.

2.4. Processing strategies
Since the study period is from January 2003 to December 2022, the cumulative SMB/mass/dynamic anomalies are relative to those in January 2003. Given that RACMO2 provides simulations of absolute SMB, the SMB anomalies are derived by removing their 1979–2008 mean (Velicogna *et al* 2014, Rignot *et al* 2019). Then, the cumulative SMB anomalies are derived by time-integrating the SMB anomalies from January 2003. Since there is no systematic bias between the GRACE and GRACE-FO time series (Velicogna *et al* 2020), the 11 month gap between them is bridged using cumulative SMB anomalies, and the remaining missing data are filled with cubic spline interpolation. Then, the gridded cumulative dynamic mass anomalies are calculated by removing the cumulative SMB anomalies from the cumulative mass anomalies (Diener *et al* 2021). The monthly time series of cumulative anomalies for an individual basin or region is calculated by integrating the values of the grids within the basin or region. The corresponding contribution to GMSL rise is determined by using the relationship that 362.5 Gt mass variation corresponds to 1 mm GMSL change (Cogley 2012). Monthly precipitation anomalies and cumulative precipitation anomalies are derived following the same approach used for RACMO2 SMB. The interannual mass (or precipitation) variation is computed using a 13 month moving average filter on the detrended time series of cumulative anomalies. Consequently, positive interannual mass (or precipitation) variation indicates higher cumulative mass (or precipitation) relative to the mean rate over the study period. In contrast, negative values indicate a reduction in mass (or precipitation).

The long-term mass change trend, or biennial mass change rate (denoted as *a* in equation (1)), is determined by least squares fitting to the time series
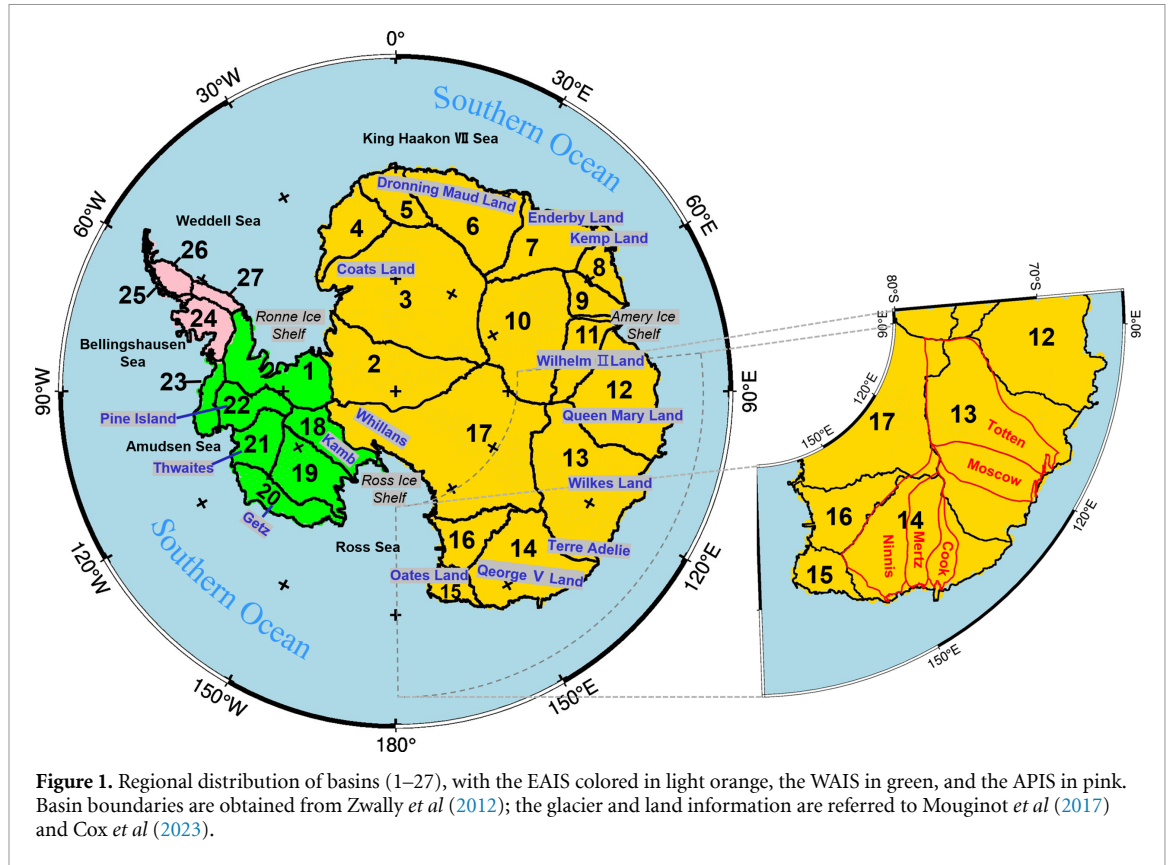
Figure 1. Regional distribution of basins (1–27), with the EAIS colored in light orange, the WAIS in green, and the APIS in pink. Basin boundaries are obtained from Zwally *et al* (2012); the glacier and land information are referred to Mouginot *et al* (2017) and Cox *et al* (2023).

of cumulative anomalies $M(t)$, using the following equation:

$$M(t_i) = a_0 + a_1 t_i + a_2 \sin(2\pi t_i) + a_3 \cos(2\pi t_i) \\ + a_4 \sin(4\pi t_i) + a_5 \cos(4\pi t_i) \tag{1}$$

where t_i is the ith time tag in years; a_0 and a_0 are the constant and biennial mass change trend (or rate); the last four terms on the right-hand represent the annual and semi-annual signals. The biennial mass change rate calculation employs time series that commence in January of the initial year and conclude in December of the second year. It should be noted that the rates for SMB and dynamic mass change are relative to the average SMB from the reference years 1979–2008.

2.5. Error estimates

The error for the cumulative mass/SMB/dynamic anomaly at a 95% confidence level (or two-sigma) is derived from the law of error propagation based on the fitting error in equation (1),

$$E_{cu(ti)} = 2\sqrt{\sigma_{a_0}^2 + t_i^2 \sigma_{a_1}^2 + \sin(2\pi t_i)^2 \sigma_{a_2}^2 + \cos(2\pi t_i)^2 \sigma_{a_3}^2 + \sin(4\pi t_i)^2 \sigma_{a_4}^2 + \cos(4\pi t_i)^2 \sigma_{a_5}^2} \tag{2}$$

where σ_{a_0}, σ_{a_1}, σ_{a_2}, σ_{a_3}, σ_{a_4}, σ_{a_5} are the one-sigma uncertainties for corresponding parameters in equation (1). The error for the mass change trend (or rate) at a 95% confidence level is derived by

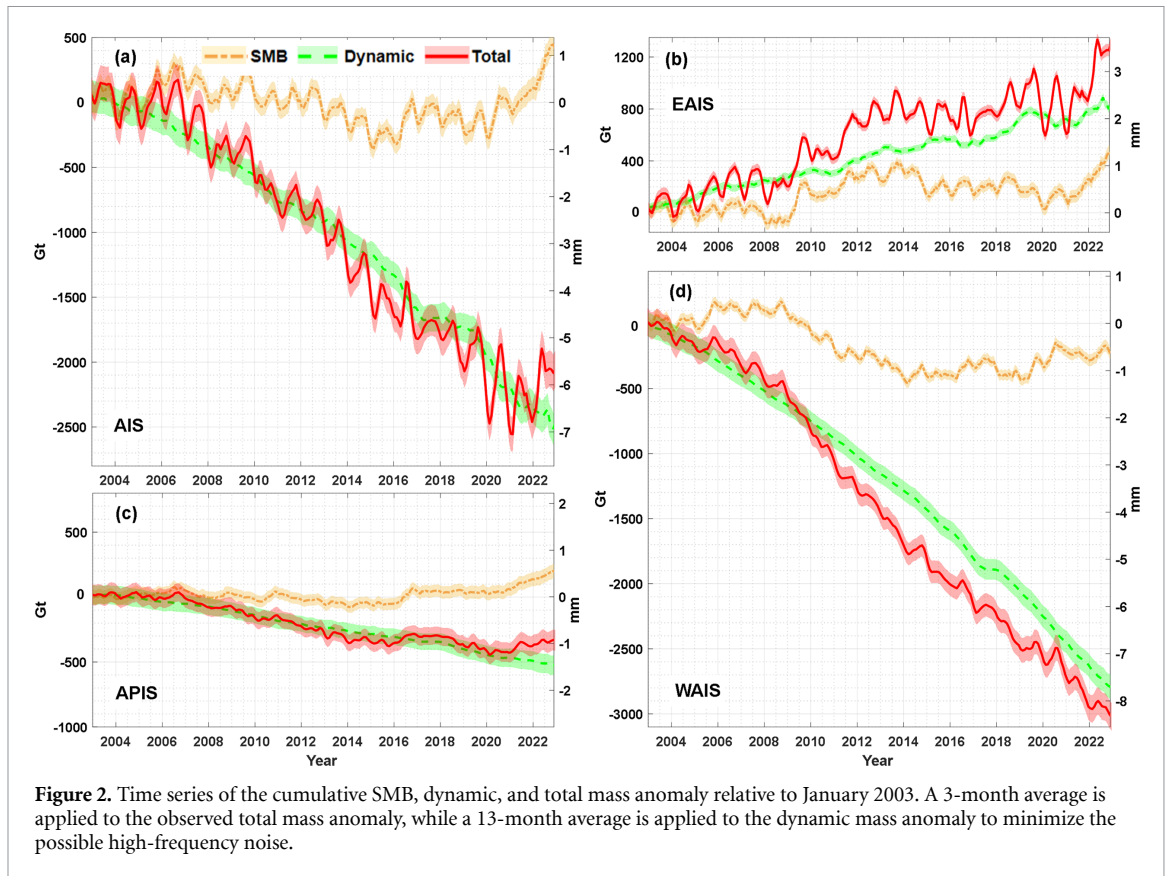$$E_{\text{trend/rate}} = 2\sqrt{\sigma_{a_1}^2 + \sigma_{\text{GIA}}^2} \tag{3}$$

where σ_{GIA} denotes the standard deviation of the GIA model, which is empirically calculated by a multimodel comparison as Smith *et al* (2020) with six GIA models from A *et al* (2013), Ivins *et al* (2013), Caron *et al* (2018), Peltier *et al* (2018), Whitehouse *et al* (2012), and Sasgen *et al* (2018). The errors of

the monthly precipitation and cumulative precipitation anomalies are also derived from the three used precipitation fields with the multimodel comparison method.

3. Results and analysis

3.1. Cumulative mass anomalies and biennial mass change rates between 2003 and 2022

The time series of cumulative mass anomalies and their contribution to GMSL for the AIS, EAIS, WAIS and APIS are depicted in figures 2(a)–(d). Results

Figure 2. Time series of the cumulative SMB, dynamic, and total mass anomaly relative to January 2003. A 3-month average is applied to the observed total mass anomaly, while a 13-month average is applied to the dynamic mass anomaly to minimize the possible high-frequency noise.

show that the AIS mass variation experienced a state of near equilibrium from 2003 to 2006, followed by a sustained mass loss until the end of 2020 with a total mass loss of 2552 ± 132 Gt. At the end of 2020, there was a reversal in the mass change state, shifting from loss to gain, which was unprecedented within the past two decades. This reversal reduced the total mass loss to 2083 ± 141 Gt by the end of 2022. In the last two years, the net mass increase is approximately 469 Gt, counterbalancing a contribution of 1.3 mm to GMSL, which has never been observed since the mid-1990s (Schröder *et al* 2019, Otosaka *et al* 2023).

Specifically, the EAIS has demonstrated sustained mass accumulation, with particularly pronounced increases from 2009 to 2012, as Boening *et al* (2012) and Shepherd *et al* (2019) reported. Most strikingly, an even more substantial mass accumulation occurred during 2021–2022 (i.e. from the beginning of 2021 to the end of 2022), and the amount is more significant than that from 2009 to 2012. Conversely, the WAIS continues to lose mass, with a cumulative loss of 3022 Gt until December 2022, contributing to a GMSL rise of approximately 8.4 ± 0.3 mm. Regarding the APIS, two significant mass accumulations occurred during 2015–2016 and 2021–2022. Notably, the mass accumulation during 2021–2022 completely offset the mass loss during 2018–2019, resulting in a seven-year cumulative mass balance from 2016 to 2022. From the cumulative SMB and dynamic mass anomalies, it is obvious that the

cumulative SMB directly modulates all the observed sharp mass gains. In contrast, the dynamic mass loss in the WAIS and APIS is the primary source of the total mass loss.

To quantify the short-term mass balance, we calculate the biennial mass change rates between 2003 and 2022 for the AIS, EAIS, WAIS, and APIS, and present them in figures 3(a)–(d). Notably, the AIS exhibited positive mass change rates during 2005–2006 and 2021–2022. In these two biennial periods, there were apparent dynamic mass losses, combined with cumulative SMB gains, particularly evident in 2021–2022. Specifically, the cumulative SMB change at 243.5 ± 29.9 Gt yr^{-1} outpaced the ice dynamics mass loss, resulting in a positive rate at 129.7 ± 69.6 Gt yr^{-1}. The total mass gain observed during 2021–2022 has never been reported before, and its magnitude of gain is unprecedentedly significant within the past two decades of GRACE/GRACE-FO records.

Notably, there are five biennial mass change rates with clear mass gains over the EAIS between 2003 and 2022, among which the highest mass gain is during 2021–2022, amounting to 273.1 ± 49.1 Gt yr^{-1}, more than five times the mass change trend of the EAIS over the past 20 years (52.7 ± 38.8 Gt yr^{-1}). The biennial mass change rate of the WAIS is -52.0 ± 32.4 Gt yr^{-1} in 2005–2006 and -87.9 ± 21.3 Gt yr^{-1} in 2019–2020, roughly equaling one-third and half of the long-term mass loss trend between 2003 and 2020
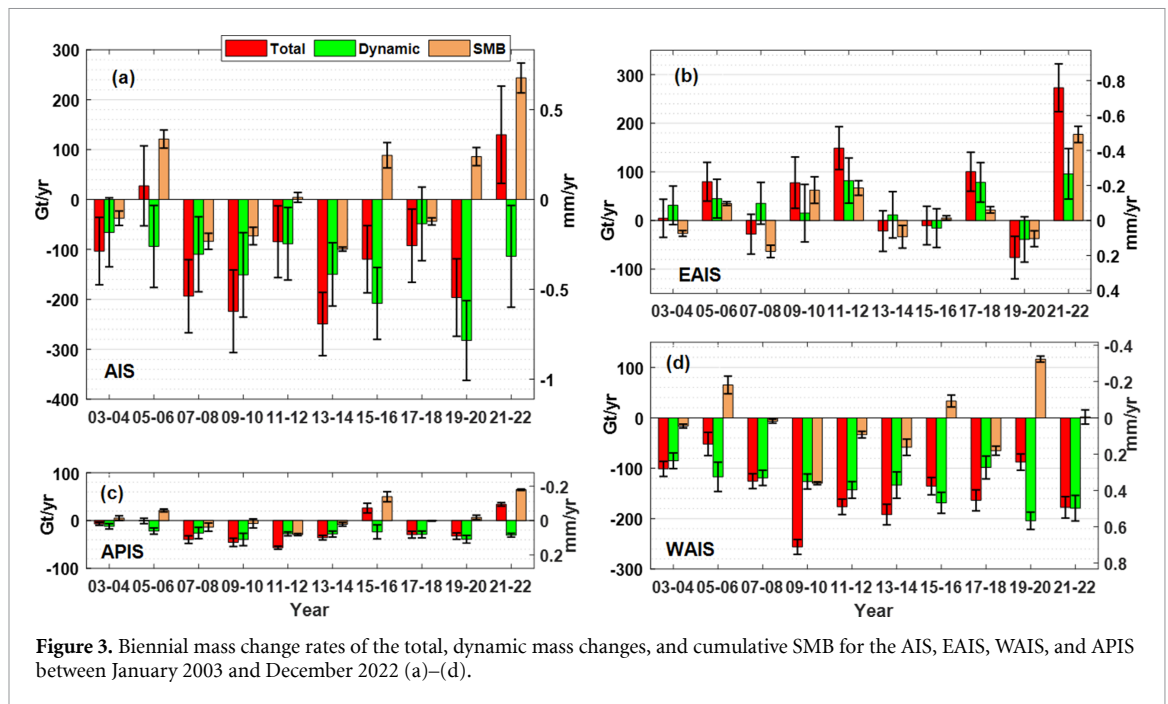
Figure 3. Biennial mass change rates of the total, dynamic mass changes, and cumulative SMB for the AIS, EAIS, WAIS, and APIS between January 2003 and December 2022 (a)–(d).

(165.9 ± 14.8 Gt yr^{-1}). Such a reduced amplitude of the mass loss for the WAIS in 2019–2020 has been rare since the late 2010s. The deceleration of mass loss in the WAIS during 2019–2020 is generally consistent with the previously observed slowdown in the Amundsen Sea sector from 2019 to 2021, as indicated by ice sheet elevation changes from multi-altimeter observations (Yue *et al* 2023). In the APIS, there was a positive mass change rate in 2015–2016, as Bodart and Bingham (2019) reported. During 2021–2022, the mass change rate again turned positive, and exceeded the previous record of mass gain observed in 2015–2016, reaching an unprecedented large magnitude within the past two decades.
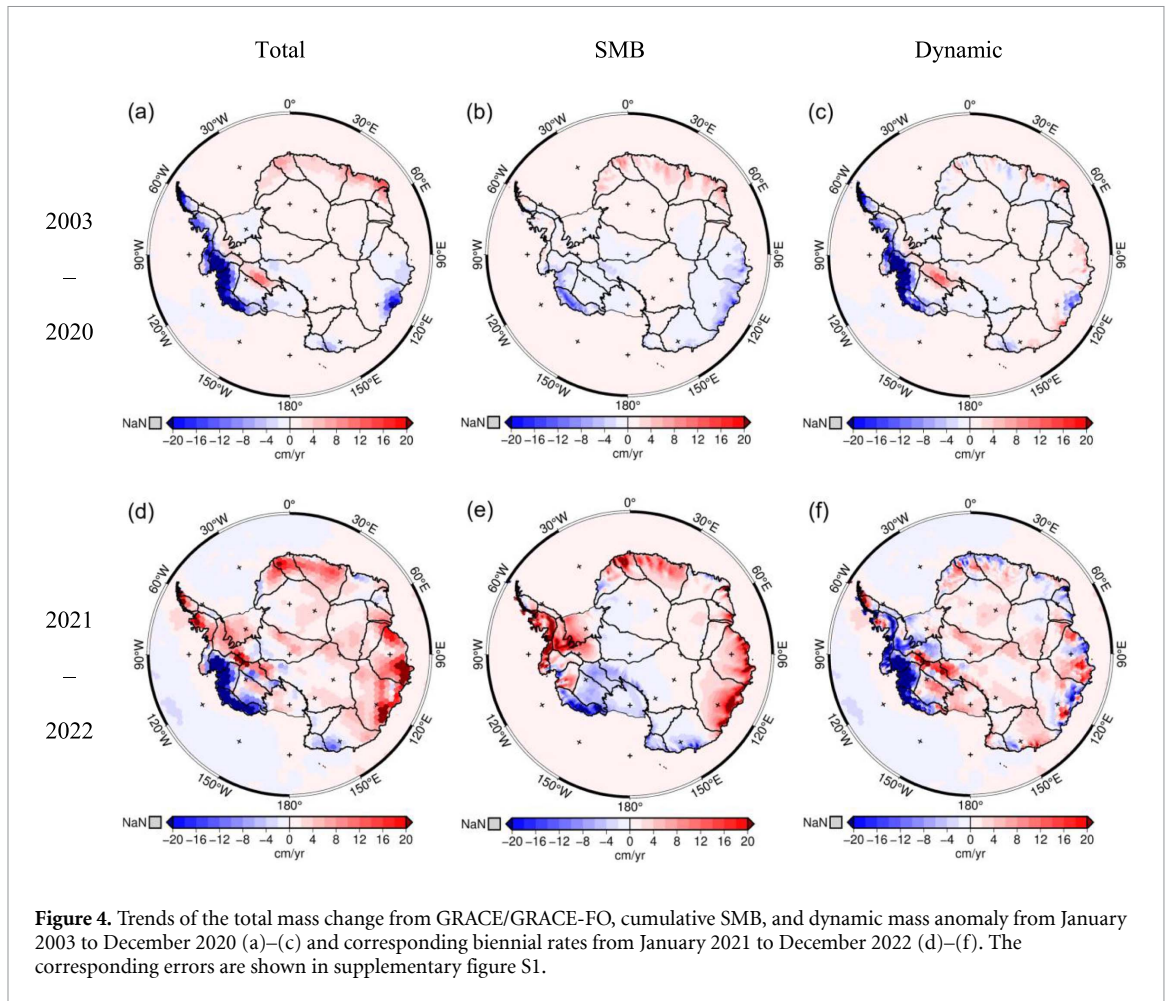
3.2. Geographical patterns for mass change trends
To investigate the mass balance before and after the observed mass gain, figure 4 depicts the geographical patterns of trends from January 2003 to December 2022 and the biennial rates of total mass changes between January 2021 and December 2022. The estimated trends and biennial rates of individual basins for the two periods are shown in supplementary table S1, in which Basin 24, 25, 26, and 27 are integrated due to the relatively small area coverage. Additionally, corresponding trends and rates for cumulative SMB/dynamic anomalies are presented to describe the direct cause of total mass change.

From 2003 to 2022, the Amundsen Sea sector and the APIS exhibited clear mass loss patterns. They are primarily driven by ice dynamic imbalances from the fast-flow glaciers of Pine Island, Thwaites, Getz (Rignot *et al* 2014), and several Bellingshausen Sea glaciers, caused by submarine melting (Mouginot *et al* 2014, Khazendar *et al* 2016) and iceberg calving (Berthier *et al* 2012). Besides, the surface mass

reduction in the Getz glacier also contributed to the total mass loss though to a lesser extent. Moreover, a prominent mass gain trend is observed in the Kamb ice streams, primarily driven by ice dynamic changes. For the EAIS, the geographical pattern of the mass change trend is more complex. The mass loss trends are evident in Queen Mary Land, George V Land, and Coats Land. In Queen Mary Land, the sustained reduction in cumulative SMB is primarily responsible for these signals. Conversely, in Coats Land and George V Land, the mass losses are predominantly driven by ice dynamic changes from the Totten, Moscow, Cook, Mertz, and Ninnis glaciers. In DML, Enderby Land, and Kemp Land, a widespread pattern of modest ice mass gain extended along much of the coastline and reached several hundred kilometers inland, closely associated with SMB accumulation. However, ice dynamic losses may offset a small portion of the mass accumulation.

The short-term mass change rates in figures 4(d)–(f) provide additional insights for the mass changes in the recent two years. Compared to the past two decades, from 2003 to 2020, the amplitude and even the sign of mass change (gain or loss) between 2021 and 2022 changed significantly over some regions. Most strikingly, there were clear mass loss signals over the APIS from 2003 to 2020. However, during 2021–2022, the mass gain was evident across most regions of the APIS, excluding the narrow peripheral areas in Basin 27. Moreover, there were significant mass gain signals over Basin 12 (Wilhelm II Land and Queen Mary Land) and Basin 13 (Wilkes Land). Basin-scale mass change rates in table S1 show that Basin 12, 13, and APIS are the top three contributors to the observed 2021–2022 mass gain over the AIS, with the biennial rates of 74.2 ± 8.0 Gt yr^{-1}, 63.2 ± 11.6 Gt yr^{-1} and

Figure 4. Trends of the total mass change from GRACE/GRACE-FO, cumulative SMB, and dynamic mass anomaly from January 2003 to December 2020 (a)–(c) and corresponding biennial rates from January 2021 to December 2022 (d)–(f). The corresponding errors are shown in supplementary figure S1.

34.1 ± 3.8 Gt yr^{-1} respectively. Besides, the mass gain rate over Basin 5–6 (DML) increased twofold from 24.0 Gt yr^{-1} to 48.1 Gt yr^{-1}. These mass gains are spatially matched with the cumulative SMB change rates, indicating that enhanced SMB accumulation is the direct cause of the observed total mass gain.

3.3. Causes for the unprecedented mass gain in the recent two years

To explore the underlying factors of the pronounced interannual variation of cumulative anomalies in total mass over the AIS, especially the observed mass gain in the recent two years, we calculate the interannual variation of cumulative anomalies in total mass and precipitation and derive corresponding cross-correlation coefficients for individual basins. The results for the focused regions of Basin 12, 13, and APIS are shown in figures 5(a)–(c).

The cross-correlation coefficients for individual basins over the AIS range from 0.47 to 0.92, with a mean value of 0.75, indicating that the interannual changes in cumulative mass anomalies are primarily driven by cumulative precipitation anomalies (Kim *et al* 2020). For Basin 12, 13, and APIS, the interannual variations between cumulative anomalies in precipitation and total mass have a high correlation (figures 5(a)–(c)). For Basin 12 (Wilhelm II Land,

Queen Mary Land) and Basin 13 (Wilkes Land), the total mass anomalies rapidly accumulated with 361 ± 23 Gt from January 2020 to December 2022, and the contemporary accumulation of precipitation anomalies was 389 ± 77 Gt. For the APIS, the total mass anomaly increase was 95 ± 47 Gt from May 2015 to December 2017, while the total mass anomaly from July 2020 to December 2022 was 111 ± 54 Gt. The corresponding increases in cumulative precipitation anomalies were 66 ± 31 Gt and 109 ± 83 Gt, respectively. Specifically, for Basin 13, two notably extreme precipitation events in March 2022 and October 2021 (supplementary figure S2) accounted for approximately 38% of the total precipitation anomalies over the three years (2020–2022). These two striking precipitation events have been linked to atmospheric rivers (Clem and Raphael 2022, Blanchard-Wrigglesworth *et al* 2023, Wille and the East Antarctica heatwave project 2023). For both Basin 12 and APIS, 26 out of 36 months (2020–2022) recorded precipitation levels exceeding the two-decade average (supplementary figure S2), indicating that the observed mass anomalies are related to the increased frequency of above-average precipitation.

As the normalized 500 hPa geopotential height serves as a crucial indicator of atmospheric pressure and motion, we present, in figures 5(d) and (e),
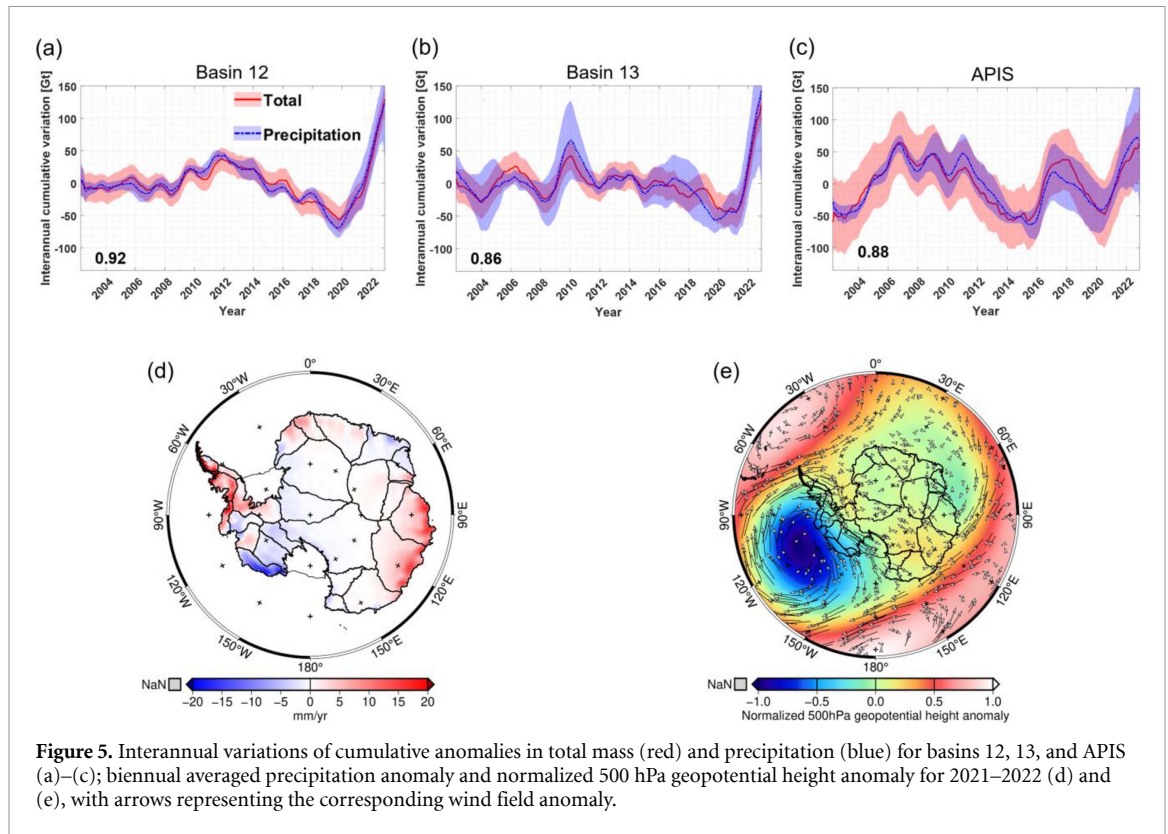
Figure 5. Interannual variations of cumulative anomalies in total mass (red) and precipitation (blue) for basins 12, 13, and APIS (a)–(c); biennial averaged precipitation anomaly and normalized 500 hPa geopotential height anomaly for 2021–2022 (d) and (e), with arrows representing the corresponding wind field anomaly.

the biennial average precipitation anomalies alongside their corresponding anomalies in the normalized 500 hPa geopotential height and wind field from the mean of MERRA-2 and ERA5 for the most recent two years, aiming to investigate the underlying driving mechanism. During 2021–2022, there was a pair of symmetrically distributed high-low pressure systems located at approximately 120° W and 60° E over the Southern Ocean. They altered the direction of the prevailing westerly winds anomalies and resulted in an excessive amount of moisture being transported toward parts of the coastal region of the EAIS, especially Basin 9–11, Basins 12, 13, the APIS, and the DML. This explains the highly enhanced precipitation in the recent two years and the significant mass accumulation depicted in figures 4(d)–(f) and 5(a)–(c). The atmospheric pressure change and its motion are essential conduits in the ocean-land mass cycle, facilitating mass transfer from the ocean to land. In other words, the modulation of the interannual mass variations of the AIS is the response to atmospheric forcing (Adusumilli *et al* 2021).

4. Conclusions

We quantified the mass change over the AIS from January 2003 to December 2022 using the GRACE/GRACE-FO and atmospheric datasets. We analyzed the biennial mass change rates to demonstrate short-term mass change. The continuous mass loss in the AIS between 2003 and 2020 was 141.8 ± 55.6 Gt yr^{-1}. Subsequently, the AIS showed

a mass gain of 129.7 ± 69.6 Gt yr^{-1} between 2021 and 2022, which was record-breaking within the past two decades of GRACE/GRACE-FO records. During this period, the mass gain over the East AIS and Antarctic Peninsula reached unprecedented levels within the past two decades, surpassing the mass loss observed in the Amundsen sector of the West AIS. Basin-scale analysis shows that the mass gain trends mainly occurred over Basin 12 (Wilhelm II Land and Queen Mary Land), Basin 13 (Wilkes Land), and the Antarctic Peninsula, at rates of 74.2 ± 8.0 Gt yr^{-1}, 63.2 ± 11.6 Gt yr^{-1} and 34.1 ± 3.8 Gt yr^{-1} respectively. The correlation analysis between the interannual variations of cumulative anomalies in precipitation and total mass suggests that the enhanced precipitation over the coastal EAIS and APIS primarily causes the observed mass gain. Further exploration indicates that the enhanced precipitation is driven by a pair of symmetrically distributed high-pressure systems over the southern ocean surrounding the Antarctic continent, which altered the direction of the prevailing westerly winds and transported more moisture toward the AIS.

Overall, our study continuously monitors the mass change of the AIS for the recent two decades and produces biennial updates of Antarctica's mass change rates in 2021–2022. The assessed biennial mass gain is unusual and offsets the previous contribution to GMSL of 1.3 mm. Our findings emphasize the impact of changing atmospheric circulation on the AIS and hold significant importance for projections of future sea-level rise.

Data availability statement

Acknowledgments

Conflict of interest

The authors declare that they have no known competing financial interests or personal relationships that could have appeared to influence the work reported in this paper.

CRediT authorship contribution statement

Wei Wang: Conceptualization, Methodology, Software, Validation, Formal analysis, Investigation, Data Curation, Writing—Original Draft, Writing—Review & Editing, Visualization. Yunzhong Shen: Methodology, Formal analysis, Investigation, Writing—Review & Editing, Funding acquisition, Supervision. Qiujie Chen: Resources, Validation. Fengwei Wang: Investigation, Writing—Review & Editing.

References

A Geruo, Wahr J and Zhong S 2013 Computations of the viscoelastic response of a 3D compressible Earth to surface loading: an application to glacial isostatic adjustment in Antarctica and Canada *Geophys. J. Int.* **192** 557–72

Adusumilli S, Fish M A, Fricker H A and Medley B 2021 Atmospheric river precipitation contributed to rapid increases in surface height of the west Antarctic ice sheet in 2019 *Geophys. Res. Lett.* **48** 1–11

Bamber J L, Westaway R M, Marzeion B and Wouters B 2018 The land ice contribution to sea level during the satellite era *Environ. Res. Lett.* **13** 063008

Bars D L, Drijfhout S and de Vries H 2017 A high-end sea level rise probabilistic projection including rapid Antarctic ice sheet mass loss *Environ. Res. Lett.* **12** 044013

Berthier E, Scambos T A and Shuman C A 2012 Mass loss of Larsen B tributary glaciers (Antarctic Peninsula) unabated since 2002 *Geophys. Res. Lett.* **39** L13501

Blanchard-Wrigglesworth E, Cox T, Espinosa Z I and Donohoe A 2023 The largest ever recorded heat wave characteristics and attribution of the Antarctic heatwave of March 2022 *Geophys. Res. Lett.* **50** e2023GL104910

Bodart J A and Bingham R J 2019 The impact of the extreme 2015–2016 El Niño on the mass balance of the Antarctic ice sheet *Geophys. Res. Lett.* **46** 13862–71

Boening C, Lebsock M, Landerer F and Stephens G 2012 Snowfall-driven mass change on the East Antarctic ice sheet *Geophys. Res. Lett.* **39** L21501

Caron L, Ivins E R, Larour E, Adhikari S, Nilsson J and Blewitt G 2018 GIA model statistics for GRACE hydrology, cryosphere, and ocean science *Geophys. Res. Lett.* **45** 2203–12

Clem K R and Raphael M N Eds 2022 Antarctica and the Southern Ocean [in "State of the Climate in 2021"] *Bull. Am. Meteorol. Soc.* **103** S307–40

Cogley J G 2012 Area of the ocean *Mar. Geod.* **35** 379–88

Cox S C et al 2023 *The GeoMAP (v.2022–08) Continent-Wide Detailed Geological Dataset of Antarctica* (PANGAEA) (https://doi.org/10.1594/PANGAEA.951482)

Davison B J, Hogg A E, Rigby R, Veldhuijsen S, van Wessem J M, van den Broeke M R, Holland P R, Selley H L and Dutrieux P 2023 Sea level rise from West Antarctic mass loss significantly modified by large snowfall anomalies *Nat. Commun.* **14** 1479

Diener T, Sasgen I, Agosta C, Fürst J J, Braun M H, Konrad H and Fettweis X 2021 Acceleration of dynamic ice loss in Antarctica from satellite gravimetry *Front. Earth Sci.* **9** 741789

Gelaro R et al 2017 The modern-era retrospective analysis for research and applications, version 2 (MERRA-2) *J. Clim.* **30** 5419–54

González-Herrero S, Vasallo F, Bech J, Gorodetskaya I, Elvira B and Justel A 2023 Extreme precipitation records in Antarctica *Int. J. Climatol.* **43** 3125–38

Hersbach H and Dee D 2016 *ERA-5 Reanalysis is in Production. ECMWF Newsletter, Number 147* (ECMWF) p 7

Ivins E R, James T S, Wahr J, Schrama O, Ernst J, Landerer F W and Simon K M 2013 Antarctic contribution to sea level rise observed by GRACE with improved GIA correction *J. Geophys. Res. Solid Earth* **118** 3126–41

Jay Z, H, Giovinetto M B, Beckley M A and Saba J L 2012 Antarctic and Greenland drainage systems (GSFC Cryospheric Sciences Laboratory) (available at: http://icesat4.gsfc.nasa.gov/cryo_data/ant_grn_drainage_systems.php)

Khazendar A, Rignot E, Schroeder D M, Seroussi H, Schodlok M P, Scheuchl B, Mouginot J, Sutterley T C and Velicogna I 2016 Rapid submarine ice melting in the grounding zones of ice shelves in West Antarctica *Nat. Commun.* **7** 13243

Kim B H, Seo K W, Eom J, Chen J L and Wilson C R 2020 Antarctic ice mass variations from 1979 to 2017 driven by anomalous precipitation accumulation *Sci. Rep.* **10** 20366

Li Z, Chao B F, Wang H S and Zhang Z Z 2022 Antarctica ice-mass variations on interannual timescale: coastal Dipole and propagating transports *Earth Planet. Sci. Lett.* **595** 117789

Loomis B D, Rachlin K E and Luthcke S B 2019 Improved Earth oblateness rate reveals increased ice sheet losses and mass-driven sea level rise *Geophys. Res. Lett.* **46** 6910–7

Loomis B D, Rachlin K E, Wiese D N, Landerer F W and Luthcke S B 2020 Replacing GRACE/GRACE-FO C30 with satellite laser ranging: impacts on Antarctic ice sheet mass change *Geophys. Res. Lett.* **47** e2019GL085488

Mouginot J, Rignot E and Scheuchl B 2014 Sustained increase in ice discharge from the Amundsen Sea Embayment, West Antarctica, from 1973 to 2013 *Geophys. Res. Lett.* **41** 1576–84

Mouginot J, Scheuchl B and Rignot E 2017 *MEaSUREs Antarctic Boundaries for IPY 2007–2009 from Satellite Radar, Version 2* (NASA National Snow and Ice Data Center Distributed Active Archive Center) (https://doi.org/10.5067/AXE4121732AD)

Oppenheimer M *et al* 2019 Sea level rise and implications for low-lying islands, coasts and communities IPCC Special Report on the Ocean and Cryosphere in a Changing Climate ed H-O Pörtner *et al* (Cambridge University Press) pp 321–445

Otosaka I N, Horwath M, Mottram R and Nowicki S 2023 Mass balances of the Antarctic and Greenland ice sheets monitored from space *Surv. Geophys.* **44** 1615–1652

Otosaka I N, Shepherd A, Ivins E R, Schlegel N-J, Amory C and van den Broeke M R 2022 Mass balance of the Greenland and Antarctic ice sheets from 1992 to 2020 *Earth Syst. Sci. Data* **15** 1–33

Peltier W R, Argus D F and Drummond R 2018 Comment on "An assessment of the ICE-6G_C (VM5a) glacial isostatic adjustment model" Purcell et al *J. Geophys. Res. Solid Earth* **123** 2019–28

Rignot E, Mouginot J, Morlighem M, Seroussi H and Scheuchl B 2014 Widespread, rapid grounding line retreat of Pine Island, Thwaites, Smith, and Kohler glaciers, West Antarctica, from 1992 to 2011 *Geophys. Res. Lett.* **41** 3502–9

Rignot E, Mouginot J, Scheuchl B, Van Den Broeke M, van Wessem M J and Morlighem M 2019 Four decades of Antarctic ice sheet mass balance from 1979–2017 *Proc. Natl Acad. Sci.* **116** 1095–103

Sasgen I, Martín-Español A, Horvath A, Klemann V, Petrie E J and Wouters B 2018 Altimetry, gravimetry, GPS and viscoelastic modeling data for the joint inversion for glacial isostatic adjustment in Antarctica (ESA STSE Project REGINA) *Earth Syst. Sci. Data* **10** 493–523

Sasgen I, Wouters B, Gardner A S, King M D, Tedesco M and Landerer F W 2020 Return to rapid ice loss in Greenland and record loss in 2019 detected by the GRACE-FO satellites *Commun. Earth Environ.* **1** 1–8

Save H 2020 *CSR GRACE and GRACE-FO RL06 Mascon Solutions V02* (University of Texas) (https://doi.org/10.15781/cgq9-nh24)

Save H, Bettadpur S and Tapley B D 2016 High-resolution CSR GRACE RL05 mascons *J. Geophys. Res. Solid Earth* **121** 7547–69

Schröder L, Horwath M, Dietrich R, Helm V, van den Broeke M R and Ligtenberg S R M 2019 Four decades of Antarctic surface elevation changes from multi-mission satellite altimetry *Cryosphere* **13** 427–49

Shepherd A, Gilbert L, Muir A S, Konrad H, McMillan M, Slater T, Briggs K H, Sundal A V, Hogg A E and Engdahl M E 2019 Trends in Antarctic ice sheet elevation and mass *Geophys. Res. Lett.* **46** 8174–83

Smith B, Fricker H A, Gardner A S, Medley B, Nilsson J and Paolo F S 2020 Pervasive ice sheet mass loss reflects competing ocean and atmosphere processes *Science* **368** 1239–42

The IMBIE team 2018 Mass balance of the Antarctic ice sheet from 1992 to 2017 *Nature* **558** 219–22

van Wessem J M *et al* 2018 Modelling the climate and surface mass balance of polar ice sheets using RACMO2: part 2: Antarctica (1979–2016) *Cryosphere* **12** 1479–98

Velicogna I *et al* 2020 Continuity of ice sheet mass loss in Greenland and Antarctica from the GRACE and GRACE follow-on missions *Geophys. Res. Lett.* **47** e2020GL087291

Velicogna I, Sutterley T C and van den Broeke M R 2014 Regional acceleration in ice mass loss from Greenland and Antarctica using GRACE time-variable gravity data *Geophys. Res. Lett.* **41** 8130–7

Whitehouse P L, Bentley M J, Milne G A, King M A and Thomas I D 2012 A new glacial isostatic adjustment model for Antarctica: calibrated and tested using observations of relative sea-level change and present-day uplift rates *Geophys. J. Int.* **190** 1464–82

Wille J and the East Antarctica heatwave project 2023 The extraordinary March 2022 East Antarctica heatwave *EGU General Assembly 2023 (Vienna, Austria, 24–28 Apr 2023)* EGU23-8107 (https://doi.org/10.5194/egusphere-egu23-8107)

Yue L *et al* 2023 Reconstructing continuous ice sheet elevation changes in the Amundsen Sea sector during 2003–2021 by merging Envisat, ICESat, CryoSat-2, and ICESat-2 multi-altimeter observations *J. Geophys. Res. Earth Surf.* **128** e2022JF007020

Zhang B, Liu L, Yao Y, van Dam T and Khan S A 2020 Improving the estimate of the secular variation of Greenland ice mass in the recent decades by incorporating a stochastic process *Earth Planet. Sci. Lett.* **549** 116518

Zwally H J, Giovinetto M B, Beckley M A and Saba J L 2012 *Antarctic and Greenland Drainage Systems* (GSFC Cryospheric Sciences Laboratory) (available at: http://icesat4.gsfc.nasa.gov/cryo_data/ant_grn_drainage_systems.php)